0026-895X/05/6806-1510–1523$20.00
MOLECULAR PHARMACOLOGY
Vol. 68, No. 6
14795/3062984
Mol Pharmacol 68:1510–1523, 2005
Printed in U.S.A.

Tweaking Agonist Efficacy at *N*-Methyl-D-aspartate Receptors by Site-Directed Mutagenesis[S]

Kasper B. Hansen, Rasmus P. Clausen, Esben J. Bjerrum, Christian Bechmann, Jeremy R. Greenwood, Caspar Christensen, Jesper L. Kristensen, Jan Egebjerg, and Hans Bräuner-Osborne

Department of Medicinal Chemistry, Danish University of Pharmaceutical Sciences, Copenhagen, Denmark (K.B.H., R.P.C., E.J.B., C.B., J.R.G., C.C., J.L.K., H.B.-O.); and Department of Molecular Neurobiology, H. Lundbeck A/S, Copenhagen, Denmark (K.B.H., C.B., J.E.)

Received May 17, 2005; accepted August 30, 2005

ABSTRACT

The structural basis for partial agonism at *N*-methyl-D-aspartate (NMDA) receptors is currently unresolved. We have characterized several partial agonists at the NR1/NR2B receptor and investigated the mechanisms underlying their reduced efficacy by introducing mutations in the glutamate binding site. Key residues were selected for mutation based on ligand-protein docking studies using a homology model of NR2B-S1S2 built from the X-ray structure of NR1-S1S2 in complex with glycine. Wild-type and mutant forms of NR2B were coexpressed with NR1 in *Xenopus laevis* oocytes and characterized by two-electrode voltage-clamp electrophysiology. By combining mutagenesis of residues His486 or Val686 with activation by differently substituted partial agonists, we introduce varying degrees of steric clash between the ligand and the two binding domains S1 and S2. In cases where ligand-protein docking predicts increased steric clashes between agonists and the residues forming the S1-S2 interface, the agonists clearly show decreased relative efficacy. Furthermore, we demonstrate that the mutation S690A affects both potency and efficacy in an agonist-specific manner. The results indicate that essential residues in the ligand binding pocket of NR2B may adopt different conformations depending on the agonist bound. Together, these data indicate that agonist efficacy at the NR2B subunit can be controlled by the extent of steric clashes between the agonist and the ligand binding domains and by ligand-dependent arrangements of residues within the binding pocket.

Ionotropic glutamate receptors mediate the greater proportion of fast excitatory neurotransmission in the mammalian brain and are divided into *N*-methyl-D-aspartate (NMDA), 2-amino-3-(3-hydroxy-5-methylisoxazol-4-yl)propionic acid (AMPA), and kainate receptors (Dingledine et al., 1999). Whereas AMPA and kainate receptors require only binding of glutamate for activation, NMDA receptors require simultaneous binding of glycine and glutamate (Cull-Candy et al., 2001). Functional NMDA receptors typically include two NR1 subunits that bind glycine and two NR2 subunits that possess glutamate binding sites (Schorge and Colquhoun, 2003). The ligand binding domain of ionotropic glutamate receptor subunits is formed by two segments, S1 and S2, separated by two transmembrane domains, as well as a membrane reentrant loop which is believed to line the pore of the ion channel (Stern-Bach et al., 1994; Paas et al., 1996). Mano et al. (1996) suggested a simple clamshell model for activation and desensitization of AMPA receptors, in which the ligand binding domains S1 and S2 form an open cleft in the absence of agonist, and when an agonist binds to the cleft, the domains close around it, leading to activation of the receptor.

X-ray structures of the ligand binding domain of the AMPA receptor GluR2 (GluR2-S1S2), alone and complexed with various agonists and antagonists, have confirmed and further refined the clamshell model (Armstrong et al., 1998; Armstrong and Gouaux, 2000; Hogner et al., 2002; Jin et al., 2003; Jin and Gouaux, 2003). In these structures, there is a correlation between the degree of ligand-induced domain closure around the agonist and the extent of receptor activation. Thus, antagonist binding results in little or no domain closure, and binding of full agonists gives rise to a higher degree of domain closure than does binding of partial agonists.

This work was supported by the Lundbeck Foundation and the Novo Nordisk Foundation.
[S] The online version of this article (available at http://molpharm.aspetjournals.org) contains supplemental material.
Article, publication date, and citation information can be found at http://molpharm.aspetjournals.org.
doi:10.1124/mol.105.014795.

ABBREVIATIONS: NMDA, *N*-methyl-D-aspartate; AMPA, 2-amino-3-(3-hydroxy-5-methylisoxazol-4-yl)propionic acid; ACBC, 1-aminocyclobutane-1-carboxylic acid; CCG, (2*S*,3*R*,4*S*)-α-(carboxycyclopropyl)glycine; HQ, homoquinolinate; AMAA, (*R*,*S*)-2-amino-2-(3-hydroxy-5-methylisoxazol-4-yl)acetic acid; NHP5G, (*R*)-2-(1-hydroxy-1*H*-pyrazol-5-yl)glycine; Cl-NHP5G, (*R*)-2-(4-chloro-1-hydroxy-1*H*-pyrazol-5-yl)glycine.

The glycine binding domain of the NMDA receptor subunit NR1 (NR1-S1S2) has been crystallized in complex with the full agonists glycine and D-serine, as well as the partial agonists D-cycloserine, 1-aminocyclopropane-1-carboxylic acid (ACPC), and 1-aminocyclobutane-1-carboxylic acid (ACBC) (Furukawa and Gouaux, 2003; Inanobe et al., 2005). These X-ray structures demonstrate that, as in GluR2, the NR1 ligand binding cleft closes upon agonist binding. However, both full and partial agonists seem to induce the same degree of domain closure in the isolated binding domain.

Because there are presently no available X-ray structures of the glutamate binding site of NR2, several previous studies have used site-directed mutagenesis to identify ligand binding residues (Williams et al., 1996; Laube et al., 1997, 2004; Anson et al., 1998; Kalbaugh et al., 2004; Chen et al., 2005; Kinarsky et al., 2005). From these studies, it can be inferred that the residues of NR2 in direct contact with glutamate share high homology with the ligand binding residues of NR1 and AMPA receptor subunits. However, the mechanisms that account for partial agonism at the glutamate binding site of NR2 subunits remain uncertain (for review, see Erreger et al., 2004).

In the present study, we explore the mechanisms underlying partial agonism at NMDA receptors. Based on receptor modeling and ligand-protein docking, we were able to introduce potential steric clashes between the ligand and residues at the interface between the two ligand-binding domains (S1 and S2) of the NMDA receptor subunit NR2B. This interference is introduced in two ways: by constricting the glutamate binding site using site-directed mutagenesis and by adding steric bulk to the agonist via substituents. In this way, we demonstrate for the first time a link between agonist efficacy at NMDA receptors and the degree to which closing of the ligand binding domains (S1 and S2) is sterically hindered. Furthermore, we investigate the effect of mutating S690A on various NMDA receptor ligands, and the findings pertaining to residue Ser690 point to a structural basis for agonist efficacy at glutamate binding site of NR2B that involves ligand-dependent arrangements of the residues of the binding pocket. Thus, the data support both steric hindrance of domain closure as well as ligand-dependent arrangements of residues govern partial agonism at the binding site of NR2B.

Materials and Methods

NMDA Receptor Ligands, DNA Constructs, and Site-Directed Mutagenesis. (*S*)-Glutamate, (2*S*,3*R*,4*S*)-α-(carboxycyclopropyl)glycine (CCG), NMDA, and glycine were obtained from Sigma-Aldrich (Munich, Germany). Homoquinolinate (HQ) was obtained from Tocris (Bristol, UK). (*R*,*S*)-2-amino-2-(3-hydroxy-5-methylisoxazol-4-yl)acetic acid (AMAA) was synthesized as described previously (Madsen et al., 1990). (*R*)-2-(1-hydroxy-1*H*-pyrazol-5-yl)glycine (NHP5G) and (*R*)-2-(4-chloro-1-hydroxy-1*H*-pyrazol-5-yl)glycine (Cl-NHP5G) were synthesized at the Danish University of Pharmaceutical Sciences (Copenhagen, Denmark) according to a previously published procedure (Cali and Begtrup, 2002), and resolved by chiral high-performance liquid chromatography (to be published elsewhere).

For expression in *Xenopus laevis* oocytes, rat NR1–1a (GenBank accession no. U11418) and rat NR2B (GenBank accession no. M91562) cDNAs were subcloned into pCI-IRES-neo and a pCI-IRES-bla vectors, respectively, containing a T7 site upstream from the 5′-untranslated region. All point mutations in NR2B were introduced using a QuikChange site-directed mutagenesis kit (Stratagene, La Jolla, CA) according to the manufacturer's protocol, and verified by DNA sequencing (MWG-Biotech, Ebersberg, Germany). Constructs used for expression in *X. laevis* oocytes were linearized by restriction enzymes to produce cRNAs, using mMessage mMachine kits (Ambion, Huntingdon, UK).

***X. laevis* Oocyte Preparation.** Oocytes were surgically removed from mature female *X. laevis* frogs anesthetized in a 0.4% 3-aminobenzoic acid ethyl ester (Sigma-Aldrich) solution for 10 to 15 min. To remove the follicle layer, the oocytes were subsequently digested with 0.5 mg/ml collagenase (type IA, Sigma-Aldrich) in OR-2 buffer (82.5 mM NaCl, 2.0 mM KCl, 1.0 mM $MgCl_2$, and 5.0 mM HEPES, pH 7.6) at room temperature for 2 to 3 h. Healthy-looking stage V–VI oocytes were selected for injection the following day. Oocytes were coinjected with cRNA encoding NR1–1a and NR2B at a 1:1 ratio and maintained at 18°C in Barth's solution [88 mM NaCl, 1.0 mM KCl, 2.4 mM $NaHCO_3$, 0.41 mM $CaCl_2$, 0.82 mM $MgSO_4$, 0.3 mM $Ca(NO_3)_2$, and 15 mM HEPES, pH 7.6] supplemented with 100 IU/ml penicillin and 100 μg/ml streptomycin (Invitrogen, Carlsbad, CA).

Electrophysiology. Two-electrode voltage-clamp recordings were performed 2 to 4 days after injection at ambient temperatures using an oocyte clamp amplifier (OC-725C; Warner Instruments, Hampden, CT) with a Digidata 1322 interface (Molecular Devices, Sunnyvale, CA). The pClamp7 suite of programs (Molecular Devices) was used to control stimulation parameters and data acquisition. Currents were low-pass filtered at 0.01 kHz and digitized at 100 Hz. The microelectrodes were fabricated from borosilicate glass capillaries (GC150TF-10; Harvard Apparatus, Holliston, MA) and pulled on a PC-10 puller (Narishige Instruments, Tokyo, Japan). Microelectrodes were filled with 3 M KCl and had 0.5- to 2.5-MΩ resistance. During recording, the oocytes were voltage-clamped at −40 mV and continuously perfused with Ca^{2+}- and Mg^{2+}-free Ringer's solution containing 115 mM NaCl, 2.5 mM KCl, 1.9 mM $BaCl_2$, and 10 mM HEPES, pH 7.6. The drugs were dissolved in Ringer's solution and applied to the oocytes by gravity-driven perfusion using a Valvebank 8 (Automate Scientific, San Francisco, CA). Because of low solubility and shift in pH of the Ringer's solution, AMAA, Cl-NHP5G, and NHP5G were applied to the oocytes at maximum concentrations of 1000 μM. Glutamate, NMDA, CCG, and HQ were used at maximum concentrations of 3000 μM. Glycine (10–20 μM) was included in the Ringer's solution at all times.

Data Analysis. Data were analyzed with Prism 4.0 (GraphPad Software, San Diego, CA). Agonist concentration-response data for individual oocytes was fitted to the Hill equation: $I = I_{max}/(1 + 10^{(\log EC_{50} - \log [A]) \times n_H})$. I_{max} is the maximum current in response to the agonist, n_H denotes the Hill coefficient, [A] is the agonist concentration, and EC_{50} is the agonist concentration that produces half-maximum response. The EC_{50} and n_H from the individual oocytes were used to calculate the mean and S.E.M. For graphical presentation, datasets from individual oocytes were normalized to the maximum current obtained from glutamate in the same recording, making it possible to calculate the mean and the S.E.M. for each data point. The averaged data points were then fitted to the Hill equation and plotted together with the resulting curve. In the figures, the concentration-response fits includes the full range of the plotted concentrations and extends the range of measured data points allowing evaluation of changes in relative maximum currents (relative I_{max}) together with changes in potencies. Relative I_{max} was calculated (unless otherwise noted) from a full concentration–response measurement as I_{max}(agonist)/I_{max}(Glu), where I_{max}(agonist) is the fitted I_{max} according to the Hill equation and I_{max}(Glu) is the maximum current obtained from glutamate in the same recording. Antagonist concentration–response data were calculated using a similar protocol, where instead of calculating the EC_{50} value, the concentration required to inhibit a glutamate-evoked response by 50% (IC_{50}) was calculated.

Molecular Modeling and Ligand-Protein Docking. A homology model of the agonized state of NR2B was constructed as follows. The crystal structure of the soluble NR1-S1S2 construct in complex

with glycine (Protein Data Bank code 1PB7) (Furukawa and Gouaux, 2003) was used as a template for the ligand binding domain of NR2B. The sequence of NR2B was aligned with NR1, truncated, and the GT linker was added to form a virtual NR2B-S1S2 construct containing residues 404 to 540 from S1 followed by the GT linker and residues 662 to 802 from S2. Residues are numbered according to the sequence of total wild-type NR2B, including the signal peptide. NR1-S1S2 contains a loop of eight residues that is disordered and missing from the currently available crystal structures (Furukawa and Gouaux, 2003). It is convenient that NR2B has a shorter sequence of seven residues in place of this loop, and the missing structural information does not affect the quality of the homology model significantly. Given the high degree of sequence conservation between NR1 and NR2B, the construct was submitted to SWISSPROT for straightforward comparative model building with first approach mode (Schwede et al., 2000).

The GluR2-S1S2:glutamate complex (Protein Data Bank code 1FTJ, chain A) (Armstrong and Gouaux, 2000) was superimposed onto the model of NR2B, and (*S*)-glutamate was copied from GluR2-S1S2 to NR2B-S1S2 as the endogenous tri-ionized ligand. The resulting NR2B-S1S2:glutamate complex was then used with the standard recommended refinement protocol in Impact 2.5 (pprep and impref) (Schrödinger, Portland, OR) to assign charges, add hydrogens, and perform a series of constrained minimizations, using the OPLS-AA forcefield. Van der Waals and electrostatic grids within a 14-Å^3 box around the ligand position were calculated on this final model with the docking code Glide 3.5 (Schrödinger); default parameters were used, apart from the scaling of nonpolar atoms of the receptor that was set to 0.9. These grids were then used for ligand docking.

The ligands NMDA, (2*S*,3*R*,4*S*)-α-CCG, HQ, (*R*)-AMAA, (*R*)-Cl-NHP5G, and (*R*)-NHP5G were submitted to Monte Carlo analysis in tri-ionized forms using the MMFFs forcefield (Halgren, 1999a,b) including GB-SA treatment of aqueous solvation in Macromodel 8.1 (Schrödinger, Portland, OR). The lowest energy conformations without intramolecular hydrogen bonding were flexibly docked with Glide 3.5 to the agonist binding site of the NR2B-S1S2 model. Default parameters were used, apart from the scaling factors of the radii of the nonpolar receptor and ligand atoms, both set to 0.9. The mutated residues were modeled by exchanging the residues in the NR2B-S1S2:glutamate model and performing a Monte Carlo search (MMFFs forcefield) of the new side chain, while restricting the backbone of the protein and allowing flexibility of sidechains within 16 Å of the ligand. The same procedure was used for simultaneously modeling residues Thr514 and Ser690. All figures of the models were prepared using PyMol software (DeLano Scientific, San Francisco, CA).

Results

Modeling the Glutamate Binding Site of NR2B. In the absence of a high-resolution X-ray structure of the NMDA receptor glutamate binding site, we have built a homology model of the NR2B ligand binding domain based on the X-ray structure of the glycine binding domain of NR1 (Furukawa and Gouaux, 2003) (see *Materials and Methods*). The purpose of this model was to help direct further studies on the structural basis for potency and efficacy of NMDA receptor agonists acting at the glutamate binding site of NR2 receptor subunits. Figure 1 shows the model of the NR2B ligand binding site with glutamate copied from the GluR2 X-ray structure (Protein Data Bank 1FTJ, chain A). The model appears in the Supplemental Data.

One of the most striking differences between the NR1 and NR2B binding sites is the switch from NR1(Trp731) to NR2(Tyr731) that controls the size of the binding pocket. In NR1, Trp731 blocks access to the area that in NR2 binds the distal γ-carboxylate of glutamate. In our model, we identify six residues from S1 and S2 (Ser512, Thr514, Arg519, Ser690, Thr691, and Asp732) that directly interact with the amino acid moiety and γ-carboxyl group of glutamate via hydrogen bonds and electrostatic interactions (Fig. 1). Figure 2A outlines the numbering of residues mutated in this study and the corresponding residues in other ionotropic glutamate receptors.

The α-ammonium group of glutamate is bound by the backbone carbonyl oxygen of Ser512 (Pro516 in NR1, Pro499 in GluR2), the side-chain hydroxyl of Thr514, and the carboxylate oxygen of Asp732 (Glu726 in GluR2). The α-carboxyl

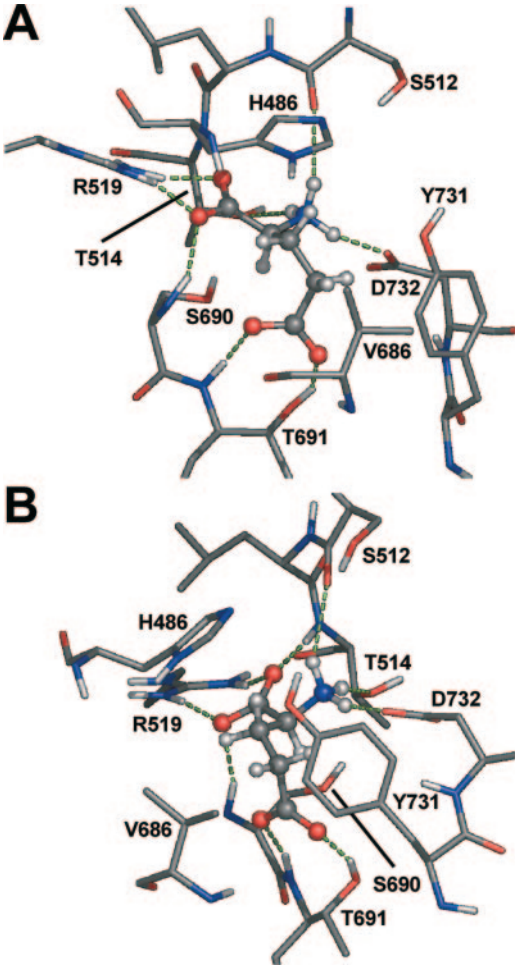

Fig. 1. Key interactions between glutamate and residues in the glutamate binding pocket of NR2B. The homology model of the glutamate binding site of NR2B was built using the glycine binding site of NR1 as a template. The GluR2-S1S2:glutamate complex (Protein Data Bank code 1FTJ, chain A) was superimposed onto the model of NR2B, and glutamate was copied from GluR2-S1S2 to NR2B-S1S2 as the endogenous ligand. Glutamate binds via hydrogen bonds and electrostatic interactions (green dotted lines) to three residues from S1 (Ser512, Thr514, Arg519) and three residues from S2 (Ser690, Thr691, Asp732). Tyr731 (Trp731 in NR1) controls whether there is access to the distal γ-carboxylate binding zone and thus whether glycine or glutamate binds to the receptor. His486 and Val686 form the entrance to a small hydrophobic pocket between the two domains (S1 and S2) in the closed conformation. Carbon (gray), nitrogen (blue), oxygen (red), and hydrogen (white) atoms of the binding pocket are presented as sticks, and atoms of glutamate are presented as ball and stick. A, the binding pocket viewed from an angle through His486 and Val686. B, the binding pocket viewed from a different angle through Tyr731. The model can be obtained as supplemental data (see Supplemental Data).

group forms a bidentate interaction with the guanidinium group of Arg519 and receives hydrogen bonds from the backbone amides of Thr514 and Ser690. The γ-carboxyl group is positioned by interactions with the backbone amide and side-chain hydroxyl of Thr691 (Val689 in NR1). The side chain of His486 (Phe484 in NR1, Tyr471 in GluR2) forms an electron-dense ring structure above the α- and β-carbon atoms that may function as a lid, restraining the space available, thereby facilitating binding of glutamate in the *S* configuration. We speculate that the size of this aromatic residue at position 486 is linked to stereospecificity, because it faces the chiral center of the ligand, and because the preference of NR2 for (*S*)-α-amino acids is generally less strict than that of GluR2. It is also noteworthy that His486 and Val686 seem to form the entrance to a small hydrophobic pocket between the two domains (S1 and S2) in the closed conformation that allow some extra space for more bulky agonists than glutamate.

Site-Directed Mutagenesis of Residues in the NR2B Ligand Binding Pocket. To verify our model of the NR2B glutamate binding site, we mutated the six residues that we predict are in direct contact with glutamate (Ser512, Thr514, Arg519, Ser690, Thr691, and Asp732). The effects of these mutations were tested on glutamate-evoked steady-state currents measured by two-electrode voltage-clamp recordings on *X. laevis* oocytes. In addition, the residues forming the entrance to the small pocket between S1 and S2 (His486 and Val686) were also mutated. The mean EC_{50} of glutamate at these NR2B mutants are listed in Table 1, and the mean concentration-response curves are displayed in Fig. 2.

T514A, R519A, T691A, and D732A mutations all give significant increases in glutamate EC_{50} (>200-fold compared with wild type) or render the receptor nonfunctional (D732A), in accordance with our model that predicts that these residues form hydrogen-bonding and electrostatic interactions with glutamate via their side chains. The charge-conserving mutation R519K renders the receptor nonfunctional, whereas the R519A mutant retains some activity (830-fold increase in EC_{50} of glutamate), suggesting that the water architecture around the monodentate salt bridge potentially formed by lysine (R519K) is unfavorable compared with the bare water-exposed carboxylate of the ligand (R519A). Mutating residues whose backbone atoms we predict bind to glutamate (S512A and S690A) does not have the same dramatic effect on glutamate potency. The EC_{50} of glutamate is reduced 2.7-fold by mutation S690A compared with at wild-type NR2B, whereas S512A increases the EC_{50} of glutamate (33-fold).

NR2B(H486L) is nonfunctional, and the EC_{50} of glutamate increases 330-fold at NR2B(H486A) over wild type. By con-

A

Total protein				Mature protein			
NR2B	**NR2A**	**NR1**	**GluR2**	**NR2B**	**NR2A**	**NR1**	**GluR2**
H486	H485	F484	Y471	H460	H466	F466	Y450
S512	S511	P516	P499	S486	S492	P498	P478
T514	T513	T518	T501	T488	T494	T500	T480
R519	R518	R523	R506	R493	R499	R505	R485
V686	V685	V684	L671	V660	V666	V666	L650
S690	S689	S688	S675	S664	S670	S670	S654
T691	T690	V689	T676	T665	T671	V671	T655
D732	D731	D732	E726	D706	D712	D714	E705

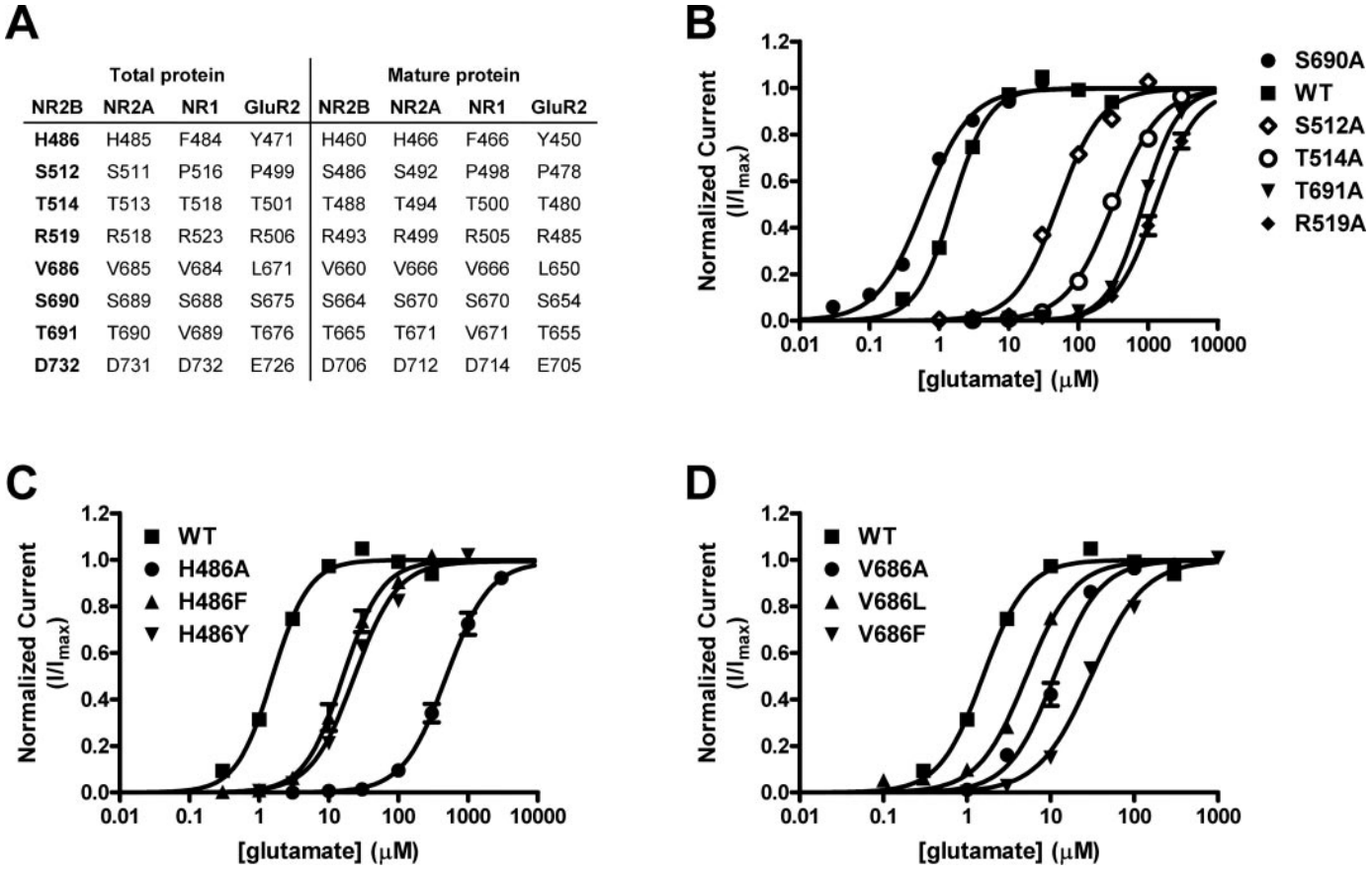

Fig. 2. A, NR2B residues mutated in this study (listed in bold) and their corresponding positions in NR2A, NR1, and GluR2. In this study, residues are numbered with respect to the amino acid sequence of the total protein including the signal peptide. Because some studies number residues with respect to the amino acid sequence of the mature protein without the predicted signal peptide these numbers are also listed here for reference. B, mean concentration–response curves for glutamate at NR1/NR2B(S690A) (●), wild-type NR1/NR2B (■), NR1/NR2B(S512A) (◇), NR1/NR2B(T514A) (○), NR1/NR2B(T691A) (▼), and NR1/NR2B(R519A) (◆). C, mean concentration–response curves for glutamate at wild-type NR1/NR2B (■), NR1/NR2B(H486A) (●), NR1/NR2B(H486F) (▲), and NR1/NR2B(H486Y) (▼). D, mean concentration–response curves for glutamate at NR1/NR2B receptors with wild type (■), V686A (●), V686L (▲), and V686F (▼) NR2B subunits. The EC_{50} values and Hill coefficients are listed in Table 1.

trast, mutations that preserve the aromatic structure only increase the EC_{50} of glutamate by 3.4-fold (H486F) and 15-fold (H486Y) demonstrating a vital role for this ring structure in coordinating agonist binding to NR2B (Table 1 and Fig. 2C).

Our model predicts that Val686 does not participate in direct binding to glutamate but rather controls the size of the entrance to the small pocket between the S1 and S2 domains. Mutation of this valine to alanine or leucine, therefore, would not be expected to produce large changes in the potency of glutamate. Therefore, mutations V686A and V686L increase the EC_{50} of glutamate by only 7.1- and 3.2-fold, respectively, whereas mutation to the more bulky phenylalanine (V686F) increases the EC_{50} of glutamate by 20-fold relative to wild type (Table 1 and Fig. 2D).

Characterization of Partial Agonists at the NR1/NR2B Receptor. To learn more about the structural basis for potency and efficacy of partial agonists at NMDA receptors, we have characterized a number of partial agonists at NR1/NR2B. Besides the partial agonist NMDA, the ligands AMAA and NHP5G, recently reported to be partial agonists (Clausen et al., 2004), and a novel NMDA receptor ligand, Cl-NHP5G, were characterized with respect to potency and efficacy of steady-state currents relative to glutamate (Tables 1 and 2; Fig. 3). Figure 3A shows the chemical structures of all the ligands used in this study. Coapplication of increasing concentrations of glutamate with each of the partial agonists demonstrated that the reduced currents elicited by AMAA, NHP5G, or Cl-NHP5G relative to glutamate are not caused by secondary effects (e.g., channel block or antagonism at the glycine site) (Fig. 3D).

NMDA, AMAA, NHP5G, and Cl-NHP5G are all analogs of aspartate; NMDA has the highest relative agonist efficacy (0.77 ± 0.01). It is noteworthy that the efficacy of NHP5G (0.61 ± 0.02) relative to that of glutamate is reduced upon chloro-substitution of the heterocycle as seen with Cl-NHP5G (0.33 ± 0.01). The relative agonist efficacy of AMAA (0.58 ± 0.02) is similar to the relative efficacy of NHP5G. Both (*R*)-aspartate and (*S*)-aspartate are partial agonists at NR1/NR2B receptors with relative agonist efficacies similar to those of NMDA (Laube et al., 2004). The results also display the deleterious effect of the bulky methyl- or chloro-substituents on the potency of AMAA (EC_{50} = 47 ± 7 μM) and Cl-NHP5G (EC_{50} = 59 ± 4 μM) compared with the potency of the unsubstituted NHP5G (EC_{50} = 14 ± 1 μM).

Modeling Partial Agonist Binding in the Ligand Binding Pocket of NR2B. AMAA, Cl-NHP5G, and NHP5G were docked to the ligand binding site of the NR2B model to examine the structural basis for their reduced efficacy compared with glutamate. Docking initially provided several potential binding modes (known as "poses"), and in the case of AMAA, two of them corresponded to low-energy conformations. In the pose shown in Fig. 4, A and B, the heterocyclic moiety overlaps with distal carboxylic acid of glutamate. The other pose (not shown) places the amino acid moiety in the same position but flips the heterocycle by ≈180°. Therefore, this pose was discarded because of the unlikely position of the distal acidic moiety. The novel NMDA receptor ligand Cl-NHP5G docked in the same way as AMAA, overlapping its amino acid moiety, heterocycle, and the negatively charged exocyclic oxygen. However, although the chloro-substituent of Cl-NHP5G is of similar size to the methyl group of AMAA, it is also more spherical and the bond length to the heterocycle is longer.

Docking NHP5G gave three poses, one of which could be discarded for same reasons as above. The other two corresponded to the same conformation, with only a slight difference in the position of the amino group. The lowest energy pose is shown in Fig. 4C.

Comparing the resulting binding modes of the ligands and given the order of efficacy (glutamate > NHP5G > Cl-NHP5G) (Fig. 3C), we surmise that reduced efficacy results from the steric bulk of the chloro-substituent of Cl-NHP5G or the methyl-substituent of AMAA protruding toward His486 and Val686 and thus serving as a wedge between S1 and S2 (Fig. 4D).

AMAA and Cl-NHP5G are Antagonists and NHP5G Is an Agonist at NR2B(H486F) and NR2B(H486Y). To evaluate how the chloro group of Cl-NHP5G and the methyl group of AMAA contribute to the observed partial agonism,

TABLE 1

Potency of agonists at the NR1/NR2B receptor with wild-type or mutant NR2B subunits

Parameters measured from steady-state currents by two-electrode voltage-clamp recordings on *X. laevis* oocytes. Mean EC_{50} ± S.E.M. was calculated from concentration-response measurements, and the mean respective Hill coefficients (n_H) are given in parentheses. *N* denotes the number of oocytes. IC_{50} values for inhibition of currents evoked by 30 μM glutamate at NR2B(H486F) and by 10 μM glutamate at NR2B(H486Y) are shown in square brackets.

NR2B mutant	EC_{50} (n_H)									
	Glutamate		NMDA		AMAA		Cl-NHP5G		NHP5G	
	μM	*N*	μM	*N*	μM	*N*	μM	*N*	μM	*N*
WT	1.6 ± 0.1 (1.7)	4	22 ± 2 (1.4)	7	47 ± 6 (1.5)	6	59 ± 4 (1.2)	6	14 ± 1 (1.4)	4
H486A	520 ± 90 (1.4)	5	>1000		N.R.		N.R.		N.R.	
H486F	5.5 ± 0.9 (1.6)	7	310 ± 20 (1.5)	5	[8.3 ± 0.3] (0.9)	7	[130 ± 10] (0.8)	6	7.1 ± 0.3 (1.0)	3
H486L	N.R.		N.D.		N.R.		N.R.		N.D.	
H486Y	24 ± 1 (1.4)	6	48 ± 1 (1.6)	4	[7.9 ± 0.2] (1.1)	7	[38 ± 1] (1.0)	6	21 ± 4 (1.2)	3
S512A	52 ± 5 (1.4)	5	760 ± 30 (2.0)	3	N.D.		N.D.		N.D.	
T514A	320 ± 20 (1.3)	5	620 ± 20 (2.0)	3	N.D.		N.D.		N.D.	
R519A	1300 ± 200 (1.5)	4	N.D.		N.D.		N.D.		N.D.	
R519K	N.R.		N.D.		N.D.		N.D.		N.D.	
V686A	11 ± 1 (1.6)	5	61 ± 3 (1.6)	5	52 ± 7 (1.2)	4	110 ± 10 (1.1)	6	22 ± 1 (1.2)	5
V686F	31 ± 3 (1.4)	5	400 ± 11 (1.6)	5	61 ± 9 (1.3)	5	140 ± 30 (1.3)	3	51 ± 9 (1.3)	4
V686L	5.1 ± 0.2 (1.5)	4	16 ± 1 (1.4)	5	87 ± 12 (1.1)	5	88 ± 19 (1.2)	4	41 ± 2 (1.7)	5
S690A	0.6 ± 0.1 (1.3)	6	2.5 ± 0.2 (1.5)	4	19 ± 1 (1.2)	5	72 ± 10 (1.5)	4	21 ± 1 (1.8)	5
T691A	840 ± 40 (1.7)	3	>3000		N.R.		N.R.		N.R.	
D732A	N.R.		N.D.		N.D.		N.D.		N.D.	

N.R., no response to 1000 μM agonist; N.D., not determined.

we examined how the relative efficacy would be affected by increasing the size of residue His486. No currents were detected when attempting to activate NR2B(H486F) and NR2B(H486Y) with AMAA and Cl-NHP5G. However, NHP5G and NMDA were still potent agonists on these mutant NR2B subunits (Table 1 and Fig. 5). Further investigation revealed that AMAA and Cl-NHP5G are antagonists at NR2B(H486F) and NR2B(H486Y).

The relative agonist efficacies of NHP5G were reduced 2.3-fold at NR2B(H486F) and 2.9-fold at NR2B(H486Y) compared with wild-type NR2B (Table 2), with small changes in agonist potencies (2.0-fold reduction (H486F) and 1.5-fold increase (H486Y) compared with the EC_{50} at wild-type NR2B) (Table 1 and Fig. 5). On the other hand, the relative agonist efficacies of NMDA were reduced by only 1.2-fold at NR2B(H486F) and NR2B(H486Y) compared with wild-type NR2B, but the EC_{50} increased 14-fold at NR2B(H486F) and 2.2-fold at NR2B(H486Y).

To probe why introducing mutations H486F or H486Y selectively convert AMAA and Cl-NHP5G to antagonists but leave NHP5G and NMDA as agonists, we introduced these mutations to our model of the NR2B ligand binding domain. The mutations were modeled by performing a Monte Carlo search while constraining the backbone of the protein and permitting movement of side chains. In the resulting models, the mutations could be accommodated in the closed conformation of the binding domain, in agreement with the fact that glutamate still activates the mutated receptors. The lowest energy conformations of the residues were used to evaluate the steric clashes between the ligands and mutated residues.

As Fig. 6 shows, the H486F mutation in S1 increases the size of the aromatic group and tilts it toward the ligands. At full domain closure, there would be increased steric crowding of the chloro-substituent of Cl-NHP5G against the rim of the aromatic ring (Fig. 6A); consequently, more space in the binding pocket is needed to accommodate this ligand. AMAA, whose methyl group occupies approximately the same position as the chloro group of Cl-NHP5G, is equally affected by this mutation. NHP5G is less affected by this mutation, pointing only a hydrogen toward Phe486 and showing a less perpendicular arrangement between its aromatic ring and that of the phenylalanine (Fig. 6B). NMDA does not occupy the same volume as NHP5G near His486, and the H486F and H486Y mutations therefore do not affect the relative efficacy to the same degree.

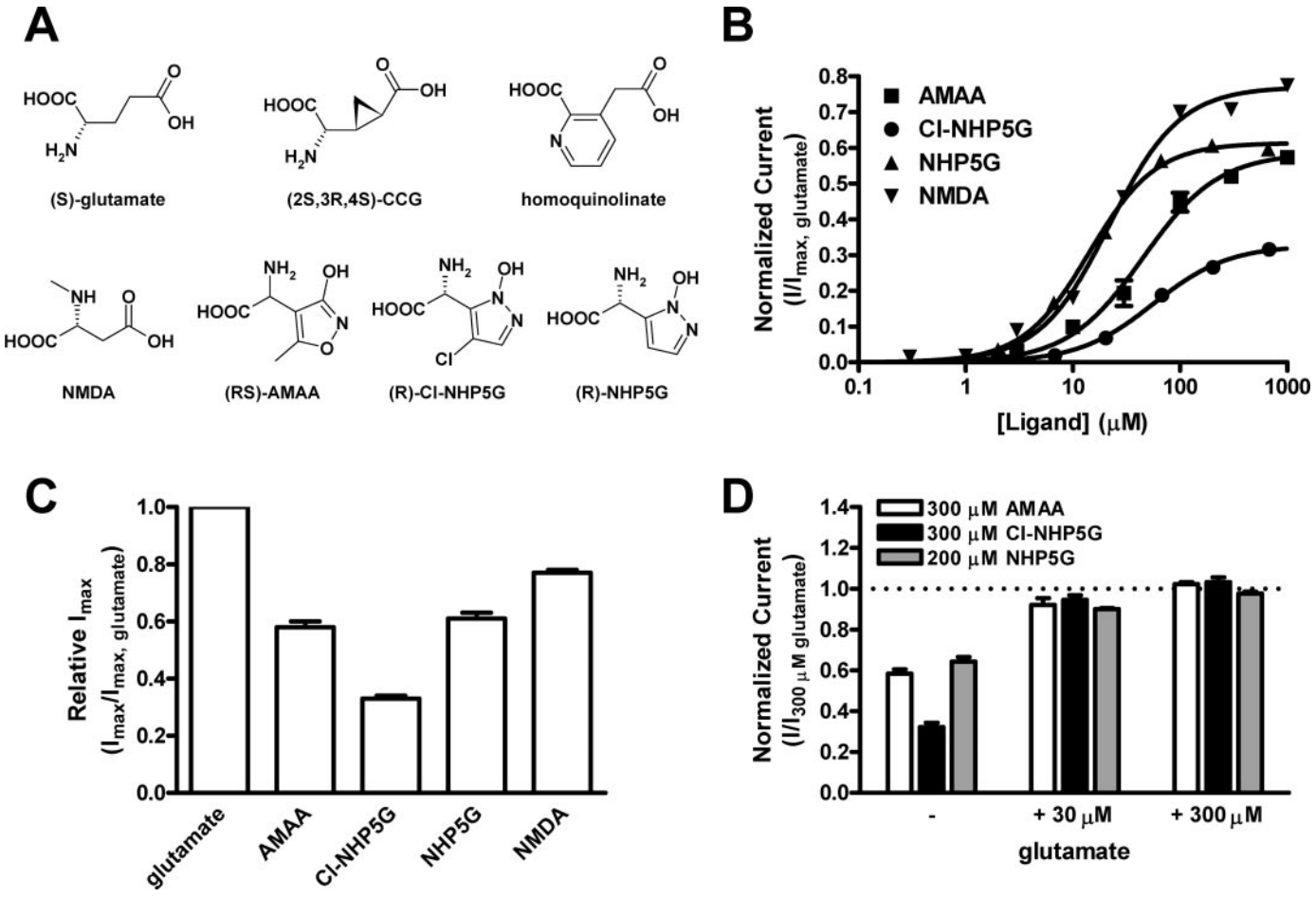

Fig. 3. A, chemical structures of the NMDA receptor ligands characterized at wild-type and mutant NR1/NR2B receptors in this study. B, mean concentration–response curves for AMAA (■), Cl-NHP5G (●), NHP5G (▲), and NMDA (▼) at the NR1/NR2B receptor. The curves are normalized to the I_{max} of glutamate. The EC_{50} values and Hill coefficients are listed in Table 1. C, relative efficacies for the four partial agonists AMAA, Cl-NHP5G, NHP5G, and NMDA at the NR1/NR2B receptor, shown here as the I_{max} of the agonist relative to the I_{max} obtained from glutamate in the same recording. The steady-state I_{max} was measured by two-electrode voltage-clamp recordings on *X. laevis* oocytes. The values are listed in Table 2. D, normalized currents evoked by AMAA (white), Cl-NHP5G (black), and NHP5G (gray) at the NR1/NR2B receptor either alone or together with 30 or 300 μM glutamate. Currents are normalized to the response evoked by 300 μM glutamate alone.

Effects of Mutating V686A, V686L, and V686F on Potency and Relative Agonist Efficacy. We assessed how AMAA and Cl-NHP5G would be affected by decreases or increases in the size of residue Val686 by characterizing NMDA, AMAA, Cl-NHP5G, and NHP5G at NR1/NR2B(V686A), NR1/NR2B(V686L) and NR1/NR2B(V686F). None of these mutations resulted in large changes in potency for AMAA, Cl-NHP5G, or NHP5G (Table 1 and Fig. 7), but they had significant effects on the relative efficacies (Table 2 and Fig. 8). The relative efficacy of NMDA was unchanged at NR1/NR2B(V686A) and NR1/NR2B(V686L), but a decrease was observed at NR1/NR2B(V686F) (Table 2 and Fig. 8). The EC_{50} of NMDA was unaffected by V686L, but was increased 2.8-fold by V686A and 18-fold by V686F (Table 1). Reducing the size of the side chain, as in NR2B(V686A), increased the relative efficacy of NHP5G but did not affect the relative efficacies of AMAA and Cl-NHP5G. Conversely, increasing the size of the side chain, as in NR2B(V686L) and NR2B(V686F), reduced the relative efficacies for all agonists (except NMDA at NR2B(V686L)), but the reduction was much more pronounced for AMAA and Cl-NHP5G than for NHP5G or NMDA. To better illustrate this observation, Fig. 8B shows the relative efficacies of NMDA, AMAA, Cl-NHP5G, and NHP5G at mutant NR2B subunits as percentage of the relative efficacy at wild-type NR2B. The order of the relative efficacies of all three partial agonists at wild type and mutant NR2B subunits was V686A $\geq$ wild type $>$ V686L $>$ V686F, which is also the reverse order of steric bulk introduced by the side chain of residue 686. It is noteworthy that the reduction in the relative efficacies of NMDA, AMAA, and NHP5G seems to be incremental with increasing size of the side chain of residue 686, whereas Cl-NHP5G is equally affected by V686L and V686F (Table 2 and Fig. 8).

As with His486, the mutations to Val686 were modeled to interpret the observed reductions in relative efficacies. Mutating Val686 in S2 to alanine, phenylalanine, and leucine represents differences in both size and nature of the steric bulk. Models of these mutated binding sites are shown in Fig. 9. The residues are positioned so that the γ-carbons of phenylalanine and leucine overlap with the γ-carbon of valine

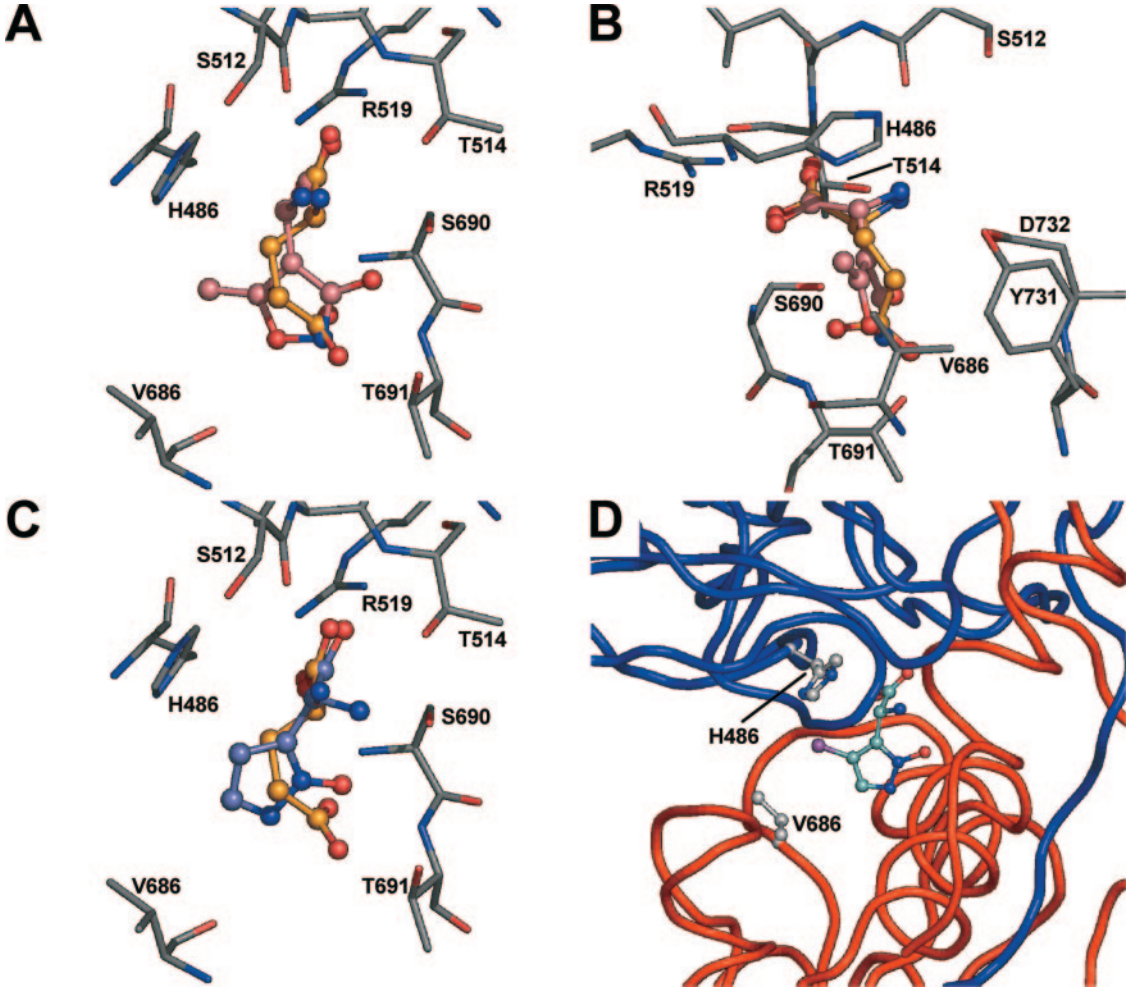

Fig. 4. Ligand-protein docking of AMAA, Cl-NHP5G, and NHP5G into the ligand binding pocket of NR2B. Carbon (gray), nitrogen (blue), and oxygen (red) atoms of the binding pocket are presented as sticks and atoms of the ligands as ball and stick. Carbon atoms of glutamate (orange), AMAA (salmon), Cl-NHP5G (cyan), and NHP5G (marine) are presented in different colors. Hydrogen atoms are omitted for clarity. A, binding of AMAA and glutamate viewed perpendicular to His486 and Val686. Tyr731 is omitted for clarity. B, binding of AMAA and glutamate viewed from an angle through His486 and Val686. The methyl-substituent protrudes directly toward the space between His486 and Val686. C, binding of NHP5G and glutamate viewed perpendicular to His486 and Val686. Tyr731 is omitted for clarity. D, binding of Cl-NHP5G, which binds similarly to AMAA, shown with NR2B-S1S2 presented in ribbon, to illustrate that the chloro-substituent (pink) of Cl-NHP5G protrudes toward His486 and Val686, acting like a wedge between S1 (blue) and S2 (red).

that protrudes into the ligand binding zone. Both phenylalanine and leucine increase the volume of this intrusion by a similar amount; however, the phenyl ring presents a plane, whereas the surface of the alkyl groups is more uneven.

The chloro-substituent of Cl-NHP5G is oriented toward these residues (Fig. 9A). Thus, phenylalanine and leucine equally affect the spherical chloro-substituent, whereas the methyl group of AMAA seems to be affected more by phenylalanine than leucine, probably because of a better mutual fit of the grooved alkyl surfaces. NHP5G is also affected, because it points its 3-position hydrogen toward the mutated residues (Fig. 9B). However, the hydrogen is much smaller and consequently does not invoke the same steric clash as a chloro or methyl group. Thus, the efficacy of NHP5G is less affected than the efficacies of AMAA or Cl-NHP5G. NHP5G is more efficacious at NR2B(V686A) than at wild-type NR2B, whereas the efficacy of neither AMAA nor Cl-NHP5G is affected by this mutation. We hypothesize that for AMAA and Cl-NHP5G, the lowered efficacy is primarily determined by the clash with His486, thus limiting an increase in efficacy at NR2B(V686A). V686A and V686L do not significantly affect either the potency or the relative efficacy of NMDA, but both are decreased by V686F. Substitution of Val686 to phenylalanine represents a significant increase in steric bulk between S1 and S2. We speculate that upon domain closure and activation of the receptor, the phenylalanine at this position in S2 will sterically clash against residues of S1 or, in case of AMAA and Cl-NHP5G, the methyl or chloro group. This

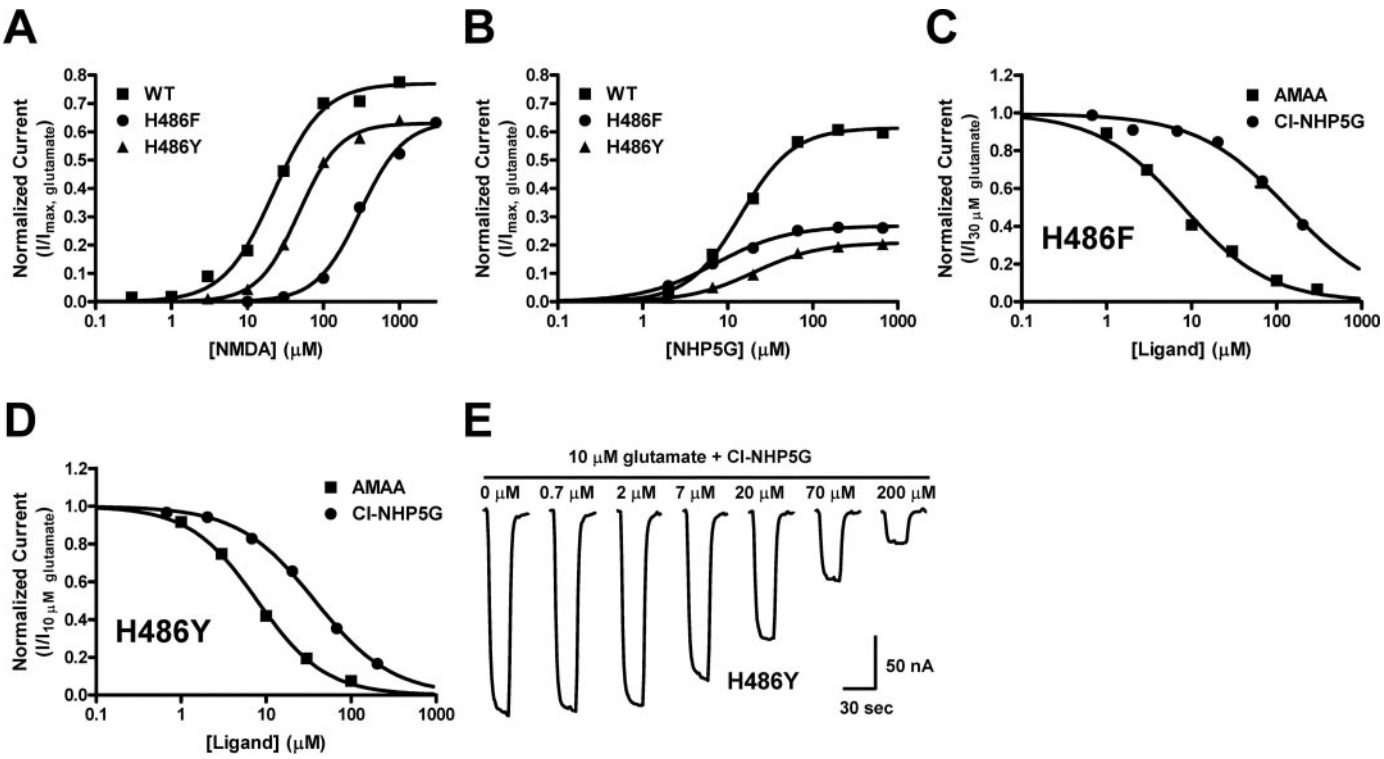

Fig. 5. A, mean concentration–response curves for NMDA at wild type NR1/NR2B (■), NR1/NR2B(H486F) (●), and NR1/NR2B(H486Y) (▲). B, mean concentration–response curves for NHP5G. The curves are normalized to the I_{max} of glutamate at the same NR2B subunit. C, mean concentration-response curves for inhibition of currents evoked by 30 μM glutamate by AMAA (■) and Cl-NHP5G (●) at NR1/NR2B(H486F) receptors. D, mean concentration-response curves for inhibition of currents evoked by 10 μM glutamate by AMAA (■) and Cl-NHP5G (●) at NR1/NR2B(H486Y) receptors. E, representative responses obtained from a two-electrode voltage-clamp recording on an *X. laevis* oocyte expressing the mutant NR1/NR2B(H486Y) receptor. Currents were evoked by coapplication of 10 μM glutamate and Cl-NHP5G (in the presence of 10 μM glycine) at the concentration indicated above each response.

TABLE 2

Relative efficacies of partial agonists at the NR1/NR2B receptor with wild type or mutant NR2B subunits

Maximum steady-state current (I_{max}) was measured by two-electrode voltage-clamp recordings on *Xenopus* oocytes. Relative I_{max} were calculated from a full concentration-response measurement as the fitted I_{max} according to the Hill equation divided by I_{max} obtained from glutamate in the same recording. Mean relative I_{max} is listed ± S.E.M. The number in parentheses (*N*) denotes the number of oocytes. Unpaired Student's *t* test was used for comparison of the relative I_{max} of a given agonist at mutant NR2B with the relative I_{max} of the same agonist at wild-type NR2B.

NR2B Mutant	Relative I_{max} (*N*)			
	NMDA	AMAA	Cl-NHP5G	NHP5G
WT	0.77 ± 0.01 (4)	0.58 ± 0.02 (32)	0.33 ± 0.01 (6)	0.61 ± 0.02 (4)
H486F	0.64 ± 0.02 (5)*	Antagonist	Antagonist	0.27 ± 0.02 (3)*
H486Y	0.63 ± 0.01 (4)*	Antagonist	Antagonist	0.21 ± 0.03 (3)*
V686A	0.75 ± 0.03 (5)	0.58 ± 0.03 (4)	0.35 ± 0.02 (6)	0.72 ± 0.01 (5)*
V686F	0.57 ± 0.01 (5)*	0.04 ± 0.01 (5)*	0.04 ± 0.01 (3)*	0.31 ± 0.02 (4)*
V686L	0.73 ± 0.02 (5)	0.25 ± 0.02 (9)*	0.08 ± 0.01 (4)*	0.39 ± 0.05 (6)*
S690A	0.93 ± 0.02 (4)*	1.15 ± 0.03 (28)*	0.67 ± 0.05 (4)*	0.78 ± 0.02 (5)*

* $P < 0.05$.

limiting of domain closure may disrupt the binding of both glutamate and NMDA and consequently lower their potency and efficacy at NR2B(V686F). This interpretation is further supported by the fact that the EC_{50} values of glutamate and NMDA are affected equally by V686F (20- and 18-fold increases, respectively).

Ligand-Dependent Effects of Mutating S690A. The 2.7-fold decrease in the EC_{50} of glutamate observed at NR2B(S690A) (Table 1 and Fig. 2B) differs from the effect described previously at NR2A(S689A), where a 1.7-fold increase in the EC_{50} of glutamate has been reported (Anson et al., 1998). The same serine residue has also been mutated to glycine in both NR2A (Chen et al., 2005) and NR2B (Laube et al., 1997) resulting in 120- and 118-fold increases in the EC_{50} of glutamate, respectively. However, glycine substitution at this position can result in altered geometry of the protein backbone, rendering the backbone amide of this residue unavailable for binding to the α-carboxy group of glutamate (Chen et al., 2005). To investigate the effect of the S690A mutation in more detail, we characterized two conformationally constrained analogs of glutamate, namely CCG and HQ (Fig. 3A), together with the four aspartate analogous (NMDA, AMAA, Cl-NHP5G, and NHP5G) at NR2B(S690A) (Figs. 10 and 11). The data are summarized in Table 3.

CCG is a potent agonist at wild-type NR2B, and S690A resulted in a slight decrease in EC_{50} (1.6-fold reduction compared with wild type NR2B), similar to the observed effect of this mutation on the EC_{50} of glutamate (2.7-fold reduction) (Figs. 2B and 10A). On the other hand, HQ and NMDA were similarly affected by S690A with 11- and 8.8-fold reductions in the EC_{50} values at NR2B(S690A) compared with at wild-type NR2B (Fig. 10, B and C). The potencies of Cl-NHP5G and NHP5G were largely unaffected by S690A, whereas the EC_{50} of AMAA was reduced by 2.5-fold (Table 3 and Fig. 10).

The relative efficacies of CCG and HQ were increased 1.1- and 1.2-fold by the S690A mutation, respectively. In fact, the relative efficacy of all agonists increased at NR2B(S690A) compared with at wild-type NR2B, with the most pronounced increases observed for AMAA (2.0-fold) and Cl-NHP5G (2.0-fold) and the smallest increase observed for CCG (Table 3 and Fig. 11).

Ligand-Induced Conformations of Residues Thr514 and Ser690. The S690A mutation mainly affected the potencies of HQ and NMDA and the efficacies of Cl-NHP5G and AMAA. To probe the role of residue Ser690, ligand-protein docking of CCG, HQ, and NMDA to the ligand binding site of the NR2B model was performed (Fig. 12). Docking CCG resulted in a pose with only minor displacements in the positions of the amino acid moiety and the distal carboxyl group from those of glutamate aligned according to the GluR2 X-ray structure (Fig. 12A). It is therefore not surprising to find that S690A has the same effect on CCG as glutamate. Docking HQ and NMDA resulted in poses with the α-carboxyl groups overlapping with that of glutamate, the protonated nitrogens near that of glutamate, and the γ-carboxyl group twisted ≈90° (Fig. 12, B and C). The nitrogen of HQ only forms a single hydrogen bond to the backbone carbonyl of Ser512, and the α-ammonium group of NMDA only two hydrogen bonds, compared with three for glutamate. According to our model, the α-ammonium group of NMDA forms hydrogen bonds to the backbone carbonyl group of Ser512 and the side-chain carboxylate of Asp732, whereas the *N*-methyl group is oriented toward Thr514. Consequently, Thr514 does not bind in the same way to glutamate as to NMDA and HQ, and this residue may adopt different conformations depending on the agonist bound. Such a difference in binding can explain why the T514A mutation affects glutamate and NMDA differently; the EC_{50} of glutamate increases 200-fold at NR2B(T514A), whereas that of NMDA increase 38-fold (Table 1). By contrast, S512A increases the EC_{50} values of glutamate and NMDA equally (33- and 34-fold, respectively). The relative I_{max} values of NMDA at NR2B(S512A) and NR2B(T514A) are 0.61 ± 0.04 (n = 3) and 0.61 ± 0.01 (n = 3).

In our model, the side-chain hydroxy group of Ser690 is near the side-chain hydroxy group of Thr514 when glutamate and CCG occupy the binding pocket. Changes in the conformation of Thr514 are therefore most likely to affect the conformation of Ser690. The agonist-dependent conformations of Thr514 and Ser690 were modeled by performing Monte Carlo searches of these side chains with NMDA

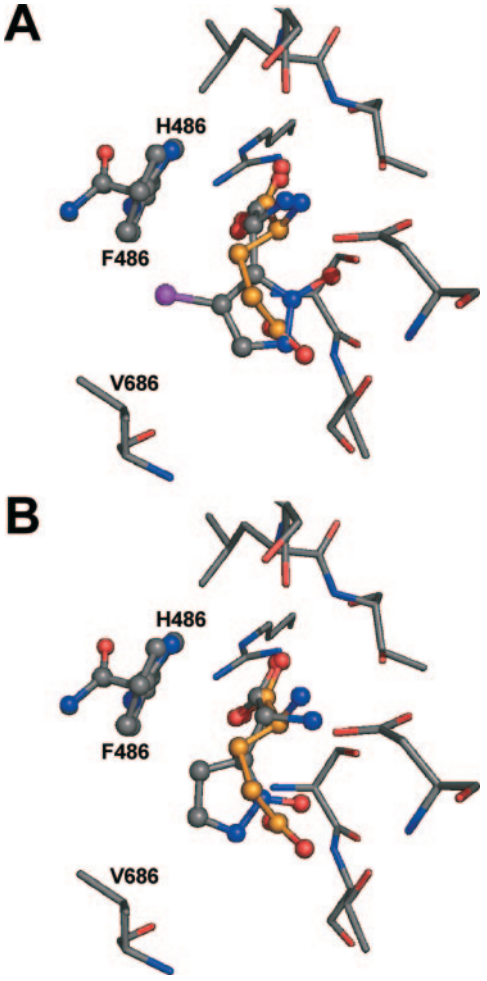

Fig. 6. Modeling of the H486F mutation in the NR2B ligand binding pocket. The H486F mutation in S1 increases the size of the aromatic group and tilts it toward the ligands. Carbon (gray), nitrogen (blue), and oxygen (red) atoms of the binding pocket are presented as sticks, and atoms of the ligands, His486, and Phe486 are presented as ball and stick. Carbon atoms of glutamate are presented in orange. Tyr731 and hydrogen atoms are omitted for clarity. A, binding of Cl-NHP5G viewed perpendicular to His486 and Val686. The chloro-substituent (pink) protrudes directly toward the space between His486 and Val686. B, binding of NHP5G viewed from the same angle.

present in the binding pocket while constraining the backbone of the protein. The results suggest that there could be alternate conformations of both Thr514 and Ser690. The lowest energy conformation in the absence of water molecules with NMDA bound is shown in Fig. 12D. This conformation creates a more favorable lipophilic environment toward the *N*-methyl group of NMDA and the aromatic ring of HQ. However, this environment is unfavorable for ligands possessing a primary amino group (i.e., glutamate and CCG). It is noteworthy that the ligand-dependent flipping proposed for Thr514 has also been observed for the corresponding Thr501 in GluR2 (Thr480 in mature GluR2) in a molecular dynamics simulation indicating a small rotation energy barrier (Arinaminpathy et al., 2002). In NR2B, the S690A mutation results in changes that are more favorable to binding of NMDA and HQ than to binding of the other agonists tested. We speculate that S690A may promote the propensity of Thr514 to flip, thereby increasing the potencies of NMDA and HQ significantly. In conjunction, the S690A mutation may simply create a water architecture more favorable to binding of NMDA and HQ.

Activity of AMAA, Cl-NHP5G, and NHP5G at NR2B(S690A). In the suggested binding modes of AMAA, Cl-NHP5G, and NHP5G, the negatively charged exocyclic oxygen is near the side-chain hydroxy group of Ser690, which is unfavorable unless this hydroxy group forms a hydrogen bond to the ligands (Fig. 4). However, such a hydrogen bond is not concordant with the unaltered potencies of the agonists at NR2B(S690A) versus wild-type NR2B (Table 3 and Fig. 10). In wild-type NR2B, we speculate that Ser690 prefers to occupy the alternative flipped conformation; instead of Ser690, a water molecule may be recruited to bind the exocyclic oxygen. In fact, the increased latitude of a water molecule at this position could be favorable for binding these ligands. When AMAA and Cl-NHP5G bind and activate the receptor, domain closure will result in increased steric crowding between His486 and the methyl group of AMAA or the chloro group of Cl-NHP5G. This increased steric crowding pushes AMAA or Cl-NHP5G, and thus the exocyclic oxygen, toward this water molecule. The more flexible architecture imparted by a water molecule at this position in NR2B(S690A) would reduce the steric clashes, and we hypothesize that this is the likely explanation for the 2.0-fold increase in the relative agonist efficacies of AMAA and Cl-NHP5G observed at NR2B(S690A) (Table 3 and Fig. 11). NHP5G does not have the same potential for clashing sterically with His486, and therefore its relative agonist efficacy increases only 1.3-fold at NR2B(S690A).

The interpretation of the effects of mutation S690A prompted a closer inspection of the published NR1 structures (Furukawa and Gouaux, 2003; Inanobe et al., 2005). The suggested flipping of Ser690 in NR2B is also observed for the corresponding serine (Ser688) in the structure of NR1-S1S2 in complex with the partial agonist ACBC (Inanobe et al., 2005) (see Supplemental Data). In NR2B, it seems likely that some flexibility is present for both Thr514 and Ser690 and that the exact positions of these two residues are determined by the structure of the bound ligand and its interplay with the surrounding water architecture. In this respect, the crystal structures of NR1 presumably display the most abundant and low-energy conformational states of these residues. We suggest that agonist potency and efficacy at NR2B are tied to ligand-induced conformational changes in Thr514 and

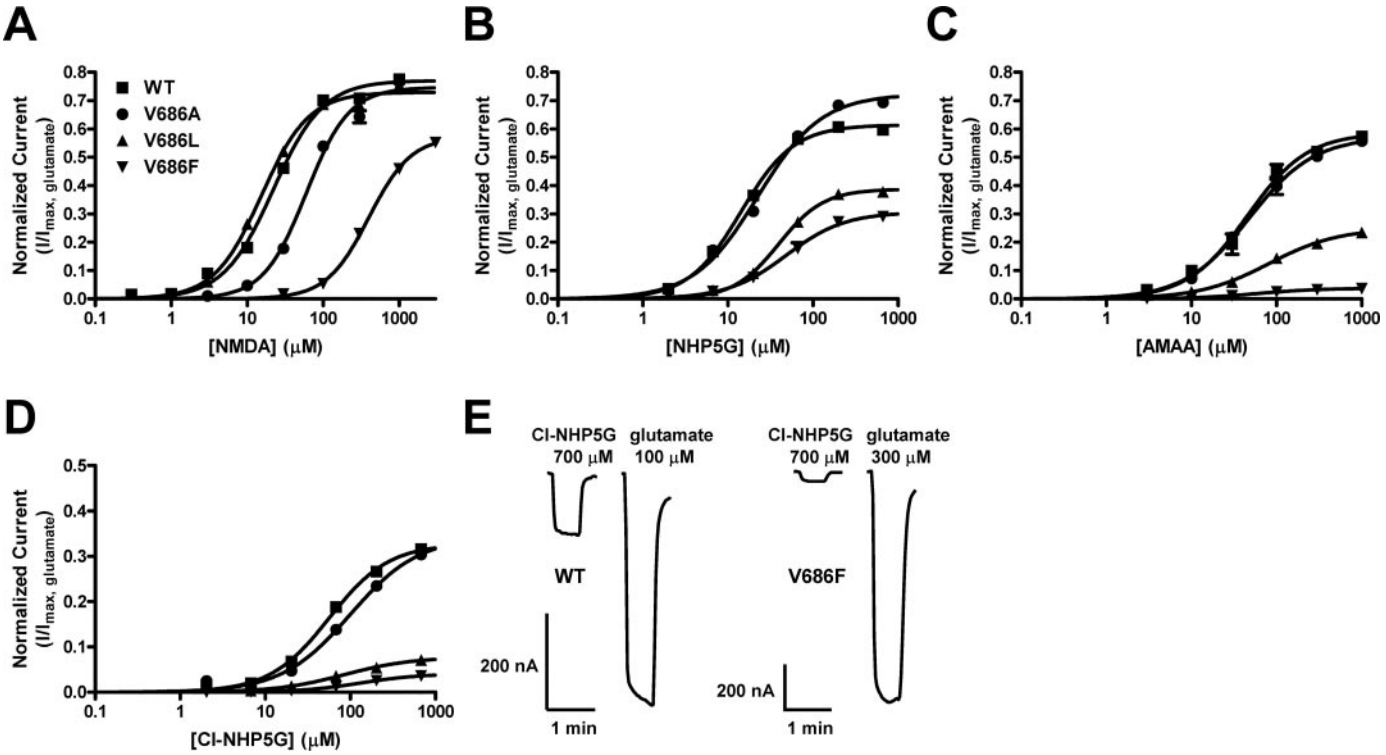

Fig. 7. A, mean concentration-response curves for NMDA. B, mean concentration-response curves for NHP5G. C, mean concentration-response curves for AMAA. D, mean concentration-response curves for Cl-NHP5G. All curves are normalized to the I_{max} of glutamate at the same NR2B subunit. The EC_{50} values and Hill coefficients are listed in Table 1. E, representative maximum currents evoked by Cl-NHP5G and glutamate at wild-type NR1/NR2B (left) or mutant NR1/NR2B(V686F) (right).

Ser690 and that the same structural features may be at work in the NR1 subunit (see Supplemental Data).

Discussion

Since the X-ray structures of the glutamate binding site of GluR2 (Armstrong et al., 1998) and glycine binding site of the NR1 subunit (Furukawa and Gouaux, 2003) were described, several studies have used these to model the glutamate binding site of NR2 (Laube et al., 2004; Chen et al., 2005; Kinarsky et al., 2005). However, because residues important for activation by glutamate were already reasonably well defined by investigations based on sequence homology (Laube et al., 1997; Anson et al., 1998), recent studies have mainly focused on identifying residues important for ligand discrimination. Work has also been carried out to determine residues important for agonist efficacy at the NR2 subunit (Kalbaugh et al., 2004; Laube et al., 2004), but none of the studies has combined homology modeling with mutational studies to address the functional effects of introducing potential steric clashes between different agonists and various residues in the binding pocket.

Steric Clashes in the Glutamate Binding Pocket of NMDA Receptors. To ensure that potential steric clashes are in fact introduced between the agonist and the residues of the domain-closed binding pocket, and not some other factor that affects efficacy, it is important not to change the underlying properties of the ligand-receptor interaction. Here, histidine is changed to phenylalanine (H486F) and tyrosine (H486Y), preserving the planar ring structure; although tyrosine introduces a distal hydroxyl group, the relative efficacies of NMDA and NHP5G are similar at NR2B(H486F) and NR2B(H486Y). The hydrophobic residue valine was mutated to alanine (V686A), leucine (V686L), and phenylalanine (V686F), preserving any potential nonpolar interactions in the binding pocket. Because we preserve the key interactions between the agonist and the binding site and predominantly change the size of the mutated residues, we conclude that the engineered steric clashes and hence short-range repulsive forces against the fully domain-closed binding site are responsible for the observed reduction in agonist efficacy.

Ligand-Dependent Conformations of Residues Thr514 and Ser690. The effect of mutation S690A on the EC_{50} of glutamate led to a closer examination of this residue under the influence of various ligands. These results led us to suggest that Thr514 and Ser690 will adopt different conformations depending on the agonist bound and that these

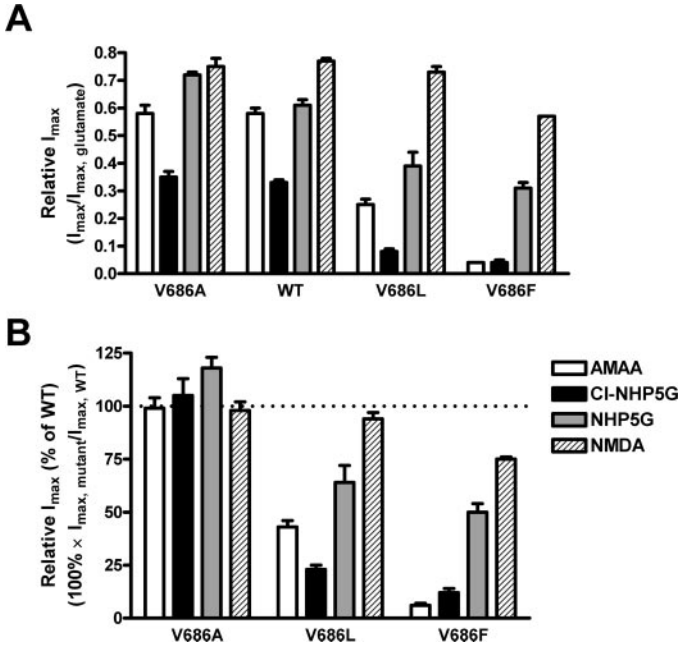

Fig. 8. A, relative efficacies for the four partial agonists AMAA (white), Cl-NHP5G (black), NHP5G (gray), and NMDA (striped) at NR1/NR2B receptors with V686A, wild type, V686L, and V686F NR2B subunits, shown here as the I_{max} of the agonist relative to the I_{max} obtained from glutamate in the same recording. The values are listed in Table 2. B, the same data as in A displayed as percentage of the relative I_{max} of the same agonist at wild-type NR1/NR2B to better visualize the more pronounced reduction in the relative efficacies of AMAA (white) and Cl-NHP5G (black) compared with NHP5G (gray) and NMDA (striped).

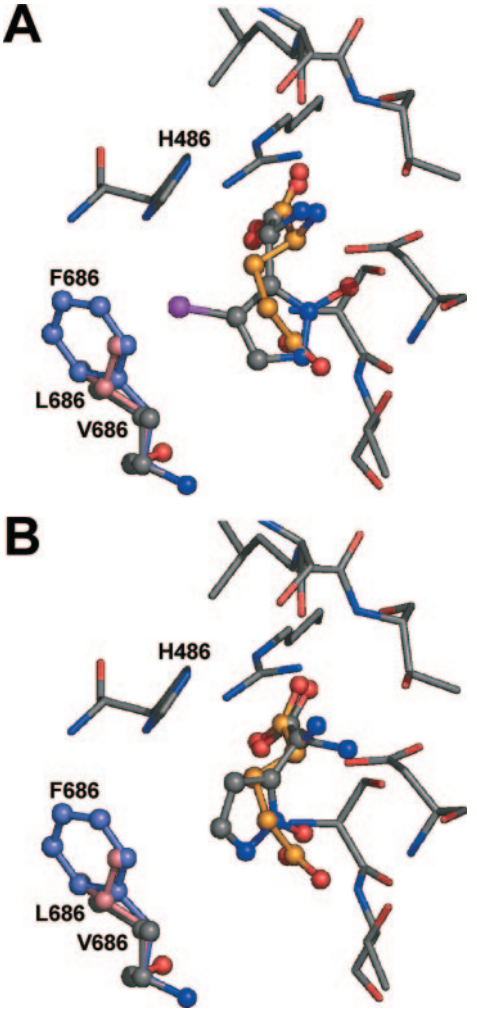

Fig. 9. Modeling of the V686A, V686L, and V686F mutations in the NR2B ligand binding pocket. The residues are positioned so that the γ-carbons of phenylalanine and leucine overlap with the γ-carbon of valine that protrudes into the ligand binding zone. Both phenylalanine and leucine increase this intrusion by a similar amount, but the phenyl ring presents a flat surface, whereas the alkyl group is more uneven. The β-carbon of alanine overlaps with that of valine and is therefore omitted for clarity. Carbon (gray), nitrogen (blue), and oxygen (red) atoms of the binding pocket are presented as sticks and atoms of the ligands, Val686, Leu686, and Phe686 as ball and stick. Carbon atoms of glutamate are presented in orange. Tyr731 and hydrogen atoms are omitted for clarity. A, binding of Cl-NHP5G viewed perpendicular to His486 and Val686. The chloro-substituent (pink) protrudes directly toward the space between His486 and Val686. B, binding of NHP5G viewed from the same angle.

ligand-induced conformations can influence potency and efficacy. Furthermore, an examination of structures of the isolated binding domain of NR1 (NR1-S1S2) suggests that similar structural features may be observed for the glycine binding site of NR1 (Furukawa and Gouaux, 2003; Inanobe et al., 2005). Functional studies at NMDA receptors have demonstrated that after agonist binding, NR1 and NR2 subunits undergo a conformational change that permits channel gating and the rate of this change is significantly slower for partial agonists than for full agonists (Banke and Traynelis, 2003). It is possible that full agonists and partial agonists induce different molecular rearrangements of residues in the binding pocket and that these different configurations could have greater or lesser probability of undergoing the conformational changes allowing channel gating on the relevant time-scales. To what extent these different rearrangements also influence domain closure remains to be determined.

Mechanisms of Partial Agonism at the NR2 Subunit of NMDA Receptors. The X-ray structures of five agonist complexes of NR1 show that the full agonists glycine and D-serine cause closing of the ligand binding domains to the same degree as the partial agonists D-cycloserine, 1-aminocyclopropane-1-carboxylic acid, and ACBC (Furukawa and Gouaux, 2003; Inanobe et al., 2005). This finding contrasts with the link between agonist efficacy and domain closure observed for the AMPA receptor subunit GluR2. The authors suggest that partial agonists might not bind as tightly as full agonists, leading to less stabilization of the closed domains (Furukawa and Gouaux, 2003; Inanobe et al., 2005). Current knowledge of partial agonism at NMDA receptors does not rule out the possibility that NR1 and NR2 subunits have different structural mechanisms determining agonist efficacy. In addition, different partial agonists (e.g., NMDA and

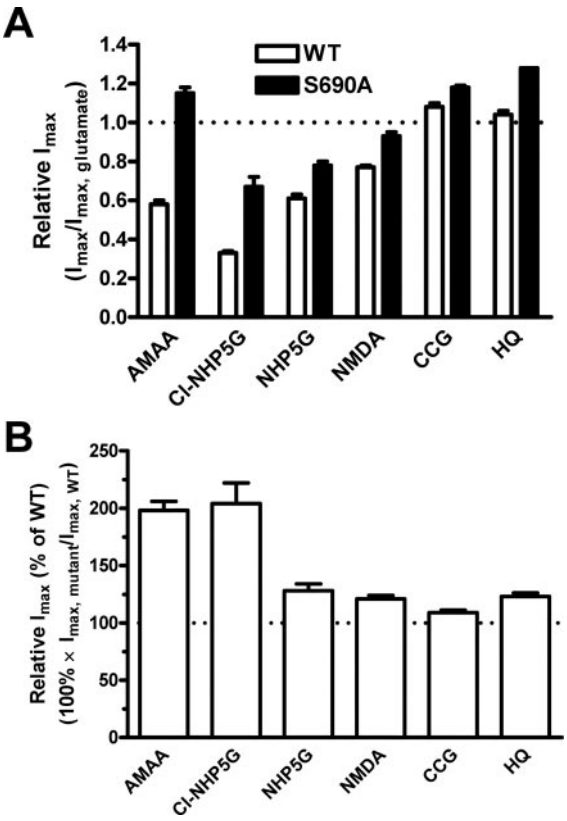

Fig. 11. A, relative efficacies for AMAA, Cl-NHP5G, NHP5G, NMDA, CCG, and HQ at wild-type NR1/NR2B (white) and mutant NR1/NR2B (S690A) (black) shown here as the I_{max} of the agonist relative to the I_{max} obtained from glutamate in the same recording. B, the same data as in A displayed as percentage of the relative I_{max} of the same agonist at wild type NR1/NR2B. The parameters are summarized in Table 3.

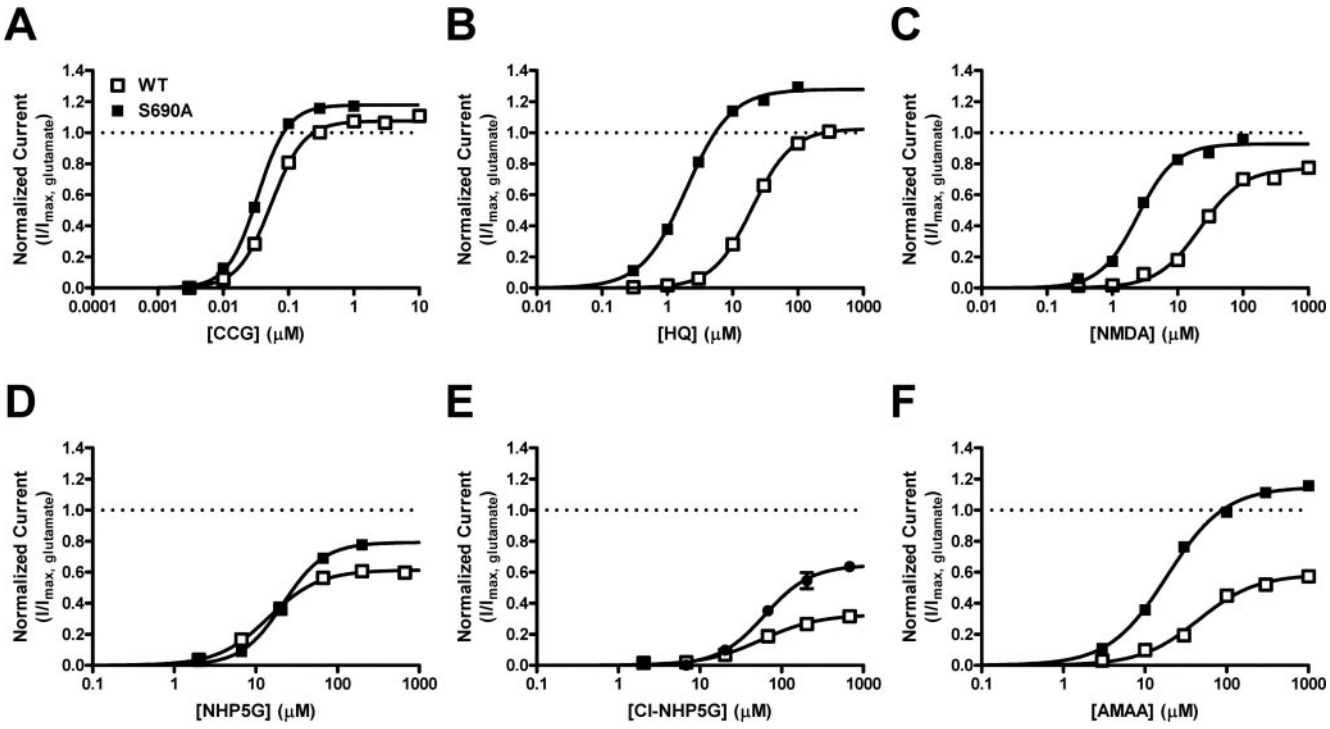

Fig. 10. Mean concentration–response curves for CCG (A), HQ (B), NMDA (C), NHP5G (D), Cl-NHP5G (E), and AMAA (F) at wild-type NR1/NR2B (□) and mutant NR1/NR2B (S690A) (■). All curves are normalized to the I_{max} of glutamate at the same NR2B subunit. The parameters are summarized in Table 3.

TABLE 3

Potency and relative efficacy of agonists at wild-type NR1/NR2B and mutant NR1/NR2B(S690A)

Parameters measured from steady-state currents by two-electrode voltage-clamp recordings on *X. laevis* oocytes. Mean EC_{50} ± S.E.M., mean respective Hill coefficients (n_H), and mean relative I_{max} ± S.E.M. are calculated as in Tables 1 and 2. The number in parentheses (*N*) denotes the number of oocytes.

Agonist	NR1/NR2B			NR1/NR2B(S690A)		
	EC_{50} (*N*)	n_H	Relative I_{max} (*N*)	EC_{50} (*N*)	n_H	Relative I_{max} (*N*)
	μM			*μM*		
Glutamate	1.6 ± 0.1 (4)	1.7		0.6 ± 0.1 (6)	1.3	
CCG	0.055 ± 0.002 (9)	1.7	1.08 ± 0.02 (9)	0.034 ± 0.001 (5)	1.9	1.18 ± 0.01 (5)
HQ	21 ± 2 (9)	1.5	1.04 ± 0.02 (9)	2.0 ± 0.1 (6)	1.3	1.28 ± 0.01 (6)
NMDA	22 ± 2 (7)	1.4	0.77 ± 0.01 (4)	2.5 ± 0.2 (4)	1.5	0.93 ± 0.02 (4)
NHP5G	14 ± 1 (4)	1.4	0.61 ± 0.02 (4)	21 ± 1 (5)	1.8	0.78 ± 0.02 (5)
Cl-NHP5G	59 ± 4 (6)	1.2	0.33 ± 0.01 (6)	72 ± 10 (4)	1.5	0.67 ± 0.05 (4)
AMAA	47 ± 6 (6)	1.5	0.58 ± 0.02 (32)	19 ± 1 (5)	1.2	1.15 ± 0.03 (28)

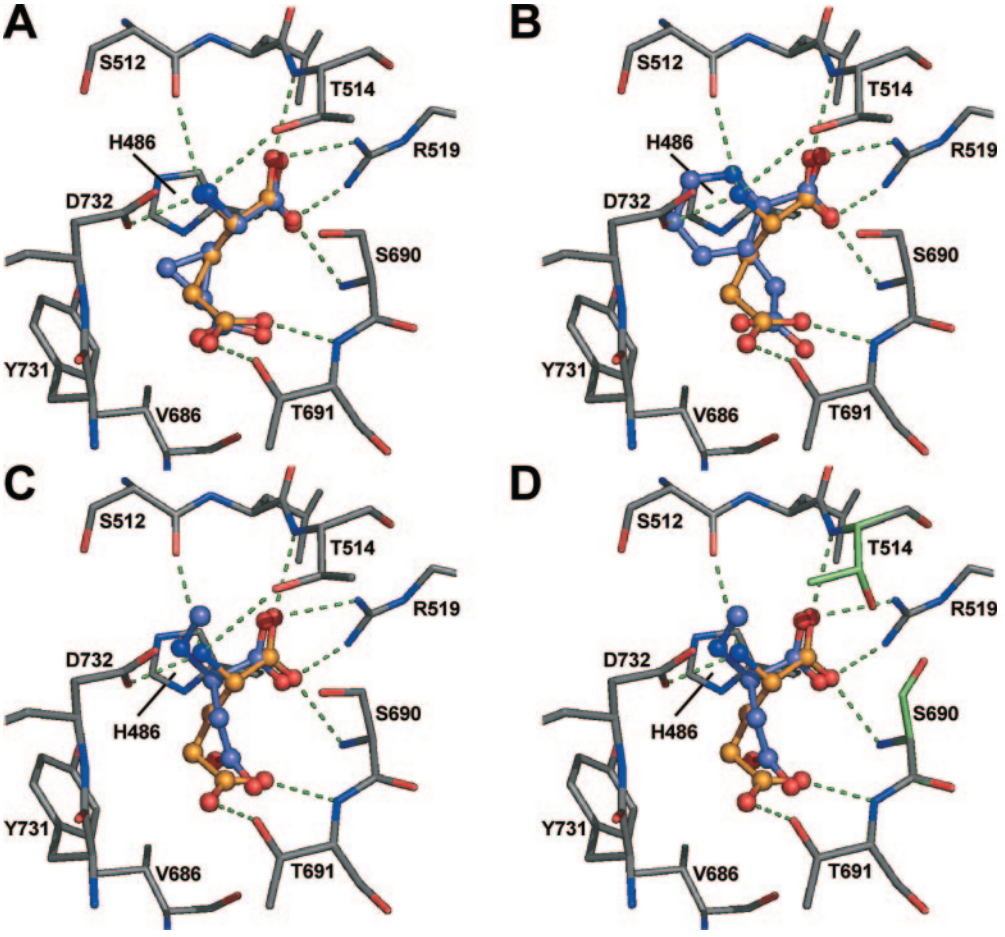

Fig. 12. Ligand-protein docking of CCG, HQ, and NMDA into the ligand binding pocket of NR2B. Carbon (gray), nitrogen (blue), and oxygen (red) atoms of the binding pocket are presented as sticks and atoms of the ligands as ball and stick. Carbon atoms of glutamate are presented in orange, and carbon atoms of CCG, HQ, and NMDA are presented in marine. All hydrogen atoms are omitted for clarity. Hydrogen bonds between glutamate and residues of the binding pocket are shown as green dotted lines. A, binding of CCG and glutamate. B, binding of HQ and glutamate. C, binding of NMDA and glutamate. D, binding of NMDA and glutamate with Thr514 and Ser690 flipped and the hydrogen bond from the side chain of Thr514 to glutamate removed. Carbon atoms of the flipped Thr514 and Ser690 side chains are presented in green.

AMAA) may have different structural bases for their reduced efficacy compared with glutamate. Finally, several mechanisms might be in play simultaneously to determine the efficacy of agonists at NMDA receptors.

The primary focus of this study was to address mechanisms accounting for partial agonism at the glutamate binding site of NR2 subunits. We demonstrate that the efficacies of the agonists investigated in the present study, AMAA, Cl-NHP5G, and NHP5G, are significantly reduced as a functional consequence of engineered steric clashes within the glutamate binding pocket of NR2B. Furthermore, we have used homology modeling to show that the critical steric interaction is introduced like a wedge between His486 from the S1 domain and Val686 from the S2 domain. Whether the wedge prevents full closure of the ligand binding domains or instead partially destabilizes the closed conformation remains to be shown. However, by linking agonist efficacy to the degree to which closing of the ligand binding domains is sterically hindered, the data presented here suggest that for some agonists, partial agonism at NMDA and AMPA receptors may arise from the same mechanism; i.e., the degree of receptor activation follows the degree of domain closure. Furthermore, we speculate that agonist potency and efficacy at NR2B may be influenced by ligand-dependent conformational changes of residues within the binding pocket and that the same structural features may be present at the NR1 subunit.

Acknowledgments

We thank Prof. Tommy Liljefors for helpful discussions and commentary on the project. We thank Dr. Ulf Madsen for generously

supplying (*R*,*S*)-AMAA. Furthermore, we acknowledge the computing resources of the Danish Center for Scientific Computing.

References

Anson LC, Chen PE, Wyllie DJ, Colquhoun D, and Schoepfer R (1998) Identification of amino acid residues of the NR2A subunit that control glutamate potency in recombinant NR1/NR2A NMDA receptors. *J Neurosci* **18:**581–589.

Arinaminpathy Y, Sansom MS, and Biggin PC (2002) Molecular dynamics simulations of the ligand-binding domain of the ionotropic glutamate receptor GluR2. *Biophys J* **82:**676–683.

Armstrong N and Gouaux E (2000) Mechanisms for activation and antagonism of an AMPA-sensitive glutamate receptor: crystal structures of the GluR2 ligand binding core. *Neuron* **28:**165–181.

Armstrong N, Sun Y, Chen GQ, and Gouaux E (1998) Structure of a glutamate-receptor ligand-binding core in complex with kainate. *Nature (Lond)* **395:**913–917.

Banke TG and Traynelis SF (2003) Activation of NR1/NR2B NMDA receptors. *Nat Neurosci* **6:**144–152.

Cali P and Begtrup M (2002) Synthesis of 1-hydroxypyrazole glycine derivatives. *Tetrahedron* **58:**1595–1605.

Chen PE, Geballe MT, Stansfeld PJ, Johnston AR, Yuan H, Jacob AL, Snyder JP, Traynelis SF, and Wyllie DJ (2005) Structural features of the glutamate binding site in recombinant NR1/NR2A *N*-methyl-D-aspartate receptors determined by site-directed mutagenesis and molecular modeling. *Mol Pharmacol* **67:**1470–1484.

Clausen RP, Hansen KB, Cali P, Nielsen B, Greenwood JR, Begtrup M, Egebjerg J, and Bräuner-Osborne H (2004) The respective *N*-hydroxypyrazole analogues of the classical glutamate receptor ligands ibotenic acid and (*RS*)-2-amino-2-(3-hydroxy-5-methyl-4-isoxazolyl)acetic acid. *Eur J Pharmacol* **499:**35–44.

Cull-Candy S, Brickley S, and Farrant M (2001) NMDA receptor subunits: diversity, development and disease. *Curr Opin Neurobiol* **11:**327–335.

Dingledine R, Borges K, Bowie D, and Traynelis SF (1999) The glutamate receptor ion channels. *Pharmacol Rev* **51:**7–61.

Erreger K, Chen PE, Wyllie DJ, and Traynelis SF (2004) Glutamate receptor gating. *Crit Rev Neurobiol* **16:**187–224.

Furukawa H and Gouaux E (2003) Mechanisms of activation, inhibition and specificity: crystal structures of the NMDA receptor NR1 ligand-binding core. *EMBO (Eur Mol Biol Organ) J* **22:**2873–2885.

Halgren TA (1999a) MMFF VI. MMFF94s option for energy minimization studies. *J Comput Chem* **20:**720–729.

Halgren TA (1999b) MMFF VII. Characterization of MMFF94, MMFF94s and other widely available force fields for conformational energies and for intermolecular-interaction energies and geometries. *J Comput Chem* **20:**730–748.

Hogner A, Kastrup JS, Jin R, Liljefors T, Mayer ML, Egebjerg J, Larsen IK, and Gouaux E (2002) Structural basis for AMPA receptor activation and ligand selectivity: crystal structures of five agonist complexes with the GluR2 ligand-binding core. *J Mol Biol* **322:**93–109.

Inanobe A, Furukawa H, and Gouaux E (2005) Mechanism of partial agonist action at the NR1 subunit of NMDA receptors. *Neuron* **47:**71–84.

Jin R, Banke TG, Mayer ML, Traynelis SF, and Gouaux E (2003) Structural basis for partial agonist action at ionotropic glutamate receptors. *Nat Neurosci* **6:**803–810.

Jin R and Gouaux E (2003) Probing the function, conformational plasticity and dimer-dimer contacts of the GluR2 ligand-binding core: Studies of 5-substituted willardiines and GluR2 S1S2 in the crystal. *Biochemistry* **42:**5201–5213.

Kalbaugh TL, VanDongen HM, and VanDongen AM (2004) Ligand-binding residues integrate affinity and efficacy in the NMDA receptor. *Mol Pharmacol* **66:**209–219.

Kinarsky L, Feng B, Skifter DA, Morley RM, Sherman S, Jane DE, and Monaghan DT (2005) Identification of subunit- and antagonist-specific amino acid residues in the *N*-methyl-D-aspartate receptor glutamate-binding pocket. *J Pharmacol Exp Ther* **313:**1066–1074.

Laube B, Hirai H, Sturgess M, Betz H, and Kuhse J (1997) Molecular determinants of agonist discrimination by NMDA receptor subunits: analysis of the glutamate binding site on the NR2B subunit. *Neuron* **18:**493–503.

Laube B, Schemm R, and Betz H (2004) Molecular determinants of ligand discrimination in the glutamate-binding pocket of the NMDA receptor. *Neuropharmacology* **47:**994–1007.

Madsen U, Ferkany JW, Jones BE, Ebert B, Johansen TN, Holm T, and Krogsgaard-Larsen P (1990) NMDA receptor agonists derived from ibotenic acid. Preparation, neuroexcitation and neurotoxicity. *Eur J Pharmacol* **189:**381–391.

Mano I, Lamed Y, and Teichberg VI (1996) A venus flytrap mechanism for activation and desensitization of α-amino-3-hydroxy-5-methyl-4-isoxazole propionic acid receptors. *J Biol Chem* **271:**15299–15302.

Paas Y, Eisenstein M, Medevielle F, Teichberg VI, and Devillers-Thiery A (1996) Identification of the amino acid subsets accounting for the ligand binding specificity of a glutamate receptor. *Neuron* **17:**979–990.

Schorge S and Colquhoun D (2003) Studies of NMDA receptor function and stoichiometry with truncated and tandem subunits. *J Neurosci* **23:**1151–1158.

Schwede T, Diemand A, Guex N, and Peitsch MC (2000) Protein structure computing in the genomic era. *Res Microbiol* **151:**107–112.

Stern-Bach Y, Bettler B, Hartley M, Sheppard PO, O'Hara PJ, and Heinemann SF (1994) Agonist selectivity of glutamate receptors is specified by two domains structurally related to bacterial amino acid-binding proteins. *Neuron* **13:**1345–1357.

Williams K, Chao J, Kashiwagi K, Masuko T, and Igarashi K (1996) Activation of *N*-methyl-D-aspartate receptors by glycine: role of an aspartate residue in the M3–M4 loop of the NR1 subunit. *Mol Pharmacol* **50:**701–708.

Address correspondence to: Hans Bräuner-Osborne, Department of Medicinal Chemistry, Danish University of Pharmaceutical Sciences, Universitetsparken 2, DK-2100 Copenhagen, Denmark. E-mail: hbo@molpharm.net